A Monte-Carlo FDTD Technique for Rough Surface Scattering

Frank D. Hastings, *Member, IEEE*, John B. Schneider, *Member, IEEE*, and Shira L. Broschat, *Member, IEEE*

Abstract—**A Monte-Carlo finite-difference time-domain (FDTD) technique is developed for wave scattering from randomly rough, one-dimensional surfaces satisfying the Dirichlet boundary condition. Both single-scale Gaussian and multiscale Pierson–Moskowitz surface roughness spectra are considered. Bistatic radar cross sections are calculated as a function of scattering angle for incident angles of 0, 45, 70, and 80 degrees measured from the vertical. The contour path FDTD method is shown to improve accuracy for incident angles greater than 45 degrees. Results compare well with those obtained using a Monte-Carlo integral equation technique.**

I. Introduction

THE finite-difference time-domain (FDTD) method was originally introduced by Yee in 1966 to calculate near-field scattering from an object in the time domain [1]. In recent years the FDTD method has achieved widespread popularity [2]–[8], and a number of extensions, modifications, and refinements have been proposed. Among other things, these allow consideration of both far-field and steady-state behavior [9]–[19].

In this paper we develop an exact numerical Monte-Carlo FDTD technique for the problem of wave scattering from randomly rough surfaces. A number of exact numerical techniques ("exact" meaning that no physical approximations are made) have been reported for rough surface scattering problems. These include finite element and finite difference methods [20]–[22] as well as integral equation techniques [23], [24]. Also, results using the FDTD method have been presented by Chan *et al.* [9], [10], Fung *et al.* [25], Schneider and Broschat [26], and Hastings *et al.* [27], [28]. The integral equation techniques have been used primarily for determining the validity of approximate models. In addition to this benchmarking application, the finite element and finite difference methods have been proposed as solutions in themselves. The goal of the present work is to develop an alternate method for determining the validity of approximate models. While an integral equation approach is more efficient for the Dirichlet surface scattering problem, volume scattering, inhomogeneous media, and complex geometries are more readily incorporated into the FDTD approach. In addition, the three-dimensional (3-D) problem is less expensive to implement using the FDTD approach, either pulsed or CW illumination can be used, propagation of both the total and scattered fields can be observed in the time domain, and a broad band of frequencies can be considered simultaneously.

Results obtained using the contour path FDTD (CPFDTD) method [11] are compared with results obtained using Yee's original FDTD algorithm. Integral equation results are included as well. Yee's algorithm, which we refer to as the uniform FDTD (UFDTD) method, uses a set of leap-frog equations that describes the fields at discrete points in a uniform grid. Because the grid is uniform and constitutive parameters can only change discretely from one evaluation point to the next, a smooth, curved interface is approximated by a discrete stair-stepped function. The CPFDTD method, introduced by Jurgens *et al.* [11], applies the integral forms of Maxwell's equations for fields near media interfaces. The paths of the contour integrals conform to the surface so that stair-stepping is eliminated.

We use both the UFDTD and CPFDTD methods to calculate the bistatic radar cross sections for one-dimensional (1-D), Dirichlet surfaces. Results are presented for randomly rough surfaces with both Gaussian and Pierson–Moskowitz surface roughness spectra. The latter spectrum represents multiscale surfaces which approximately model the sea surface [29]. The Dirichlet problem corresponds to two types of wave scattering: acoustic scattering from pressure-release surfaces such as the air-sea interface and TM_z polarized electromagnetic wave scattering from perfectly conducting surfaces.

Initially it was thought that the CPFDTD method would give better results for all incident angles for the same number of points per wavelength (ppw). For many surfaces, however, it was found that the staircase approximation causes significant errors only for incident angles greater than approximately 45 degrees. The error is largest in the backscatter direction but is still small relative to the strongest incoherent scatter. Since the true backscattered energy is large for incident angles near normal, the error is negligible for these cases.

In the next section, implementation of the Monte-Carlo FDTD method is described. Included are brief discussions of the original Yee algorithm, CPFDTD method, absorbing boundary conditions, incident field, surface generation, far-field conversion, and Monte-Carlo averaging technique. Equations are given in terms of electric and magnetic field

Manuscript received August 25, 1993; revised November 21, 1994. This work was supported in part by the Office of Naval Research Code 3210A and by the National Science Foundation Grants ECS9058186 and ECS9253547.

The authors are with the School of Electrical Engineering and Computer Science, Washington State University, Pullman, WA 99164-2752 USA.

IEEE Log Number 9414659.

0018–926X/95$04.00 © 1995 IEEE

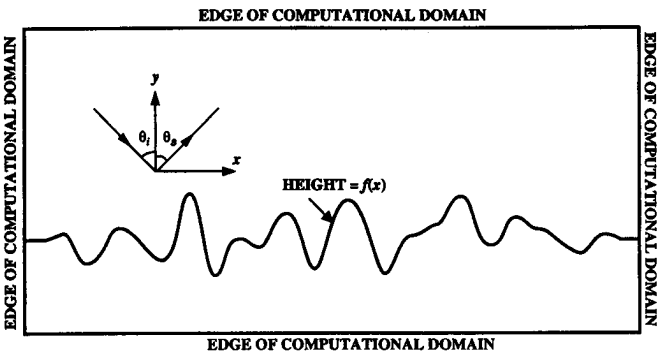

Fig. 1. Problem geometry including FDTD computational grid. Only scattered fields propagate on the grid, and the incident field is introduced at the surface.

components only, but can be adapted easily to their acoustic analogs. In Section III, numerical results are presented.

II. Implementation

The problem geometry is shown in Fig. 1. Each surface realization is set within a computational grid that conforms to the scattered field FDTD formulation [8]. This formulation was found to perform as well as the total field approach, yet it is much easier to implement. Only scattered fields are computed; the incident field is introduced by means of the boundary condition at the surface—that is, the tangential scattered $\boldsymbol{E}$-field is set equal to the negative of the incident field. Buffer zones are included at the surface edges for the absorbing boundary conditions (see Section II-C).

Our review of the UFDTD method is brief. For a detailed explanation, the reader is referred to [1]–[8]. The CPFDTD time-stepping equations are derived specifically for a rough surface geometry such as shown in Fig. 1. For additional information on the CPFDTD method, the reader is referred to [11].

A. The UFDTD Method

The UFDTD method is based on the differential forms of Ampere's and Faraday's laws. For the Dirichlet 1-D surface TM_z problem, only the E_z-, H_x-, and H_y-field components are nonzero, and Maxwell's curl equations take the following form

$$\frac{\partial E_z}{\partial t} = \frac{1}{\epsilon}\left[\frac{\partial H_y}{\partial x} - \frac{\partial H_x}{\partial y}\right] \tag{1}$$

$$\frac{\partial H_x}{\partial t} = \frac{1}{\mu}\frac{\partial E_z}{\partial y} \tag{2}$$

$$\frac{\partial H_y}{\partial t} = \frac{1}{\mu}\frac{\partial E_z}{\partial x} \tag{3}$$

where ϵ and μ are the permittivity and permeability, respectively. For the Yee algorithm [1], these equations are approximated using central differences. In two dimensions, the $\boldsymbol{E}$- and $\boldsymbol{H}$-field quantities are spatially arranged as shown in Fig. 2(a) to give central differences with second-order accuracy. Each grid point is specified by coordinates $(x, y) = (i\Delta x, j\Delta y)$, where the grid spacing is $\Delta = \Delta x = \Delta y$. For simplicity, we refer to points with the reference indexes (i, j). In addition to a spatial separation, there is a temporal separation: the $\boldsymbol{H}$-field components are evaluated a half time step later than the $\boldsymbol{E}$-field components. Using Fig. 2, (1)–(3) can be rewritten in such a way that all future values can be expressed in terms of previous values. We obtain

$$E_z^n(i,j) = E_z^{n-1}(i,j) + \frac{\delta t}{\epsilon\Delta}\cdot\left[\left(H_y^{n-(1/2)}\left(i+\frac{1}{2},j\right) - H_y^{n-(1/2)}\left(i-\frac{1}{2},j\right)\right) - \left(H_x^{n-(1/2)}\left(i,j+\frac{1}{2}\right) - H_x^{n-(1/2)}\left(i,j-\frac{1}{2}\right)\right)\right] \tag{4}$$

$$H_x^{n+(1/2)}\left(i,j+\frac{1}{2}\right) = H_x^{n-(1/2)}\left(i,j+\frac{1}{2}\right) - \frac{\delta t}{\mu\Delta}[E_z^n(i,j+1) - E_z^n(i,j)] \tag{5}$$

$$H_y^{n+(1/2)}\left(i+\frac{1}{2},j\right) = H_y^{n-(1/2)}\left(i+\frac{1}{2},j\right) + \frac{\delta t}{\mu\Delta}[E_z^n(i+1,j) - E_z^n(i,j)] \tag{6}$$

where δt equals one time step and $\Delta x = \Delta y = \Delta$ equals one grid space. Time is indicated by the superscript and position is given parenthetically. The algorithm is stepped through time, computing a field component at each grid point based on the values of the neighboring field components at previous times. Equation (4), for example, shows how E_z at a particular time step, n, is computed from its own value at a previous time step, $n-1$, and from surrounding magnetic field values at the previous half time step, $n-\frac{1}{2}$. A half time step later, $n+\frac{1}{2}$, this value of E_z is used to find H_x and H_y as described by (5) and (6). This process is repeated to obtain propagation of the fields.

B. The CPFDTD Method

Several conformal techniques have been proposed. Each involves altering the grid to better fit a curved surface. In the method used in this work based on the contour path approach of Jurgens *et al.* [11], the grid is deformed only near a media interface, leaving the remainder of the grid in its rectangular form. Madsen and Ziolkowski [12] present a modified finite volume technique that creates time-stepping equations for any convex polygonal grid. Consequently, it is possible to apply the technique to the same partially distorted grid structure used in the contour path method. Yee *et al.* [13] introduced a technique that employs two meshes; one is an undistorted master mesh, and the other is a conformal mesh used in the vicinity of curved surfaces. Other methods distort the grid globally. One scheme proposed by Holland [16] and used by Fusco [15] implements a curvilinear form of the FDTD equations on a grid distorted to fit the shape of the scatterer. The same type of grid is used by Shankar *et al.* [14]; however, the time-stepping equations are developed from a computational fluid dynamics approach. McCartin and Dicello [17] propose an extension of the control region approach to the

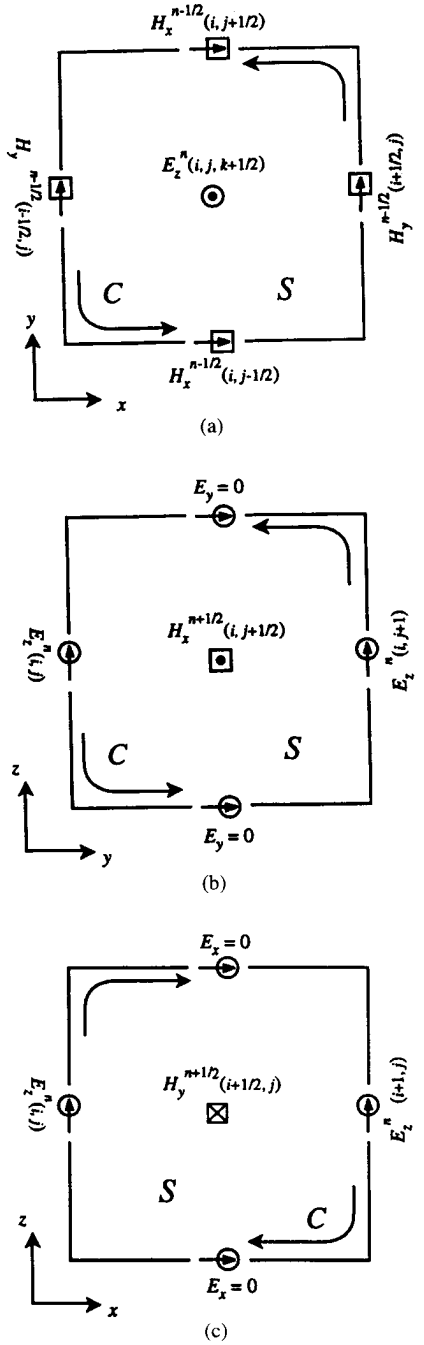

Fig. 2. Contours used to approximate the integral forms of Faraday's and Ampere's laws. Each figure represents a plane of the 3-D FDTD grid. Orientations are indicated by the adjoining axes. (a) Ampere contour for E_z. (b) Faraday contour for H_x. (c) Faraday contour for H_y.

FDTD formulation. A rigorous comparison of the efficiency, advantages, and disadvantages of each method is not yet available in the literature, although comparisons have been made of the dispersive properties of some of the techniques [18].

The CPFDTD method is based on the integral forms of Ampere's and Faraday's laws

$$\int_C \boldsymbol{H} \cdot d\boldsymbol{l} = \epsilon \frac{d}{dt} \int_S \boldsymbol{E} \cdot d\boldsymbol{s} \tag{7}$$

$$\int_C \boldsymbol{E} \cdot d\boldsymbol{l} = -\mu \frac{d}{dt} \int_S \boldsymbol{H} \cdot d\boldsymbol{s} \tag{8}$$

where, as before, only E_z, H_x, and H_y are nonzero for the TM_z problem. It is possible to evaluate (7) and (8) over the contours shown in Fig. 2 which represent grid cells located away from a media interface. The contour of Fig. 2(a) is used to evaluate (7), and the contours of Fig. 2(b) and (c) are used to evaluate (8). In each case, a contour C surrounds a square area $S = \Delta^2$. In general, each contour includes four field quantities, but for the problem considered here, E_x, E_y, and H_z are zero. The field value at the center of S is assumed to be the average value over this area. Also, the field values on each segment of C are assumed to be constant. With these simplifications it is easy to show that (7) and (8) reduce to (4)–(6). Hence, there is no difference between the UFDTD and CPFDTD methods for grid points away from a media interface.

The difference in the contour path implementation becomes apparent when it is applied near an interface. Contours can be deformed to follow a surface profile, leading to equations more accurate than those used in the UFDTD method. The undistorted contours that would extend beneath the surface are truncated to form new contours bounded on one edge by the surface. For the 1-D surface problem, a surface profile $f(x)$ does not vary with z, so for each value of x, the surface height is constant for all z. For this reason, contours lying in the z-x or z-y planes are truncated uniformly by the surface, producing new rectangular contours. The Faraday contours—that is, those contours associated with Faraday's law (8)—shown in Fig. 2(b) and (c) are of this type, and the manner in which they are deformed is shown in Fig. 3(a) and (b), respectively. The top portion of Fig. 3 shows one edge of each of the Faraday contours (the dashed lines) in addition to a surface profile. As will be discussed later, we define each surface profile by a set of real numbers corresponding to the surface height at discrete horizontal locations. Therefore, piecewise linear segments are used to depict the surface in Fig. 3. The bottom portion of Fig. 3 shows the geometry of the two new contours. Using the appropriate deformations and the fact that the tangential component of the electric field vanishes on a perfectly conducting surface, (8) can be used to solve for the magnetic fields in terms of previously obtained values

$$H_x^{n+(1/2)}\left(i, j+\frac{1}{2}\right) = H_x^{n-(1/2)}\left(i, j+\frac{1}{2}\right) - \frac{\delta t}{\mu l_y} E_z^n(i, j+1) \tag{9}$$

$$H_y^{n+(1/2)}\left(i, j+\frac{1}{2}\right) = H_y^{n-(1/2)}\left(i, j+\frac{1}{2}\right) + \frac{\delta t}{\mu l_x} E_z^n(i+1, j) \tag{10}$$

or

$$H_y^{n+(1/2)}\left(i+\frac{1}{2}, j\right) = H_y^{n-(1/2)}\left(i+\frac{1}{2}, j\right) - \frac{\delta t}{\mu l_x} E_z^n(i, j) \tag{11}$$

where l_y and l_x are dimensions of the truncated contour as shown in Fig. 3. Equation (10) corresponds to Fig. 3(b) with truncation of the contour occurring on the "left" side as shown.

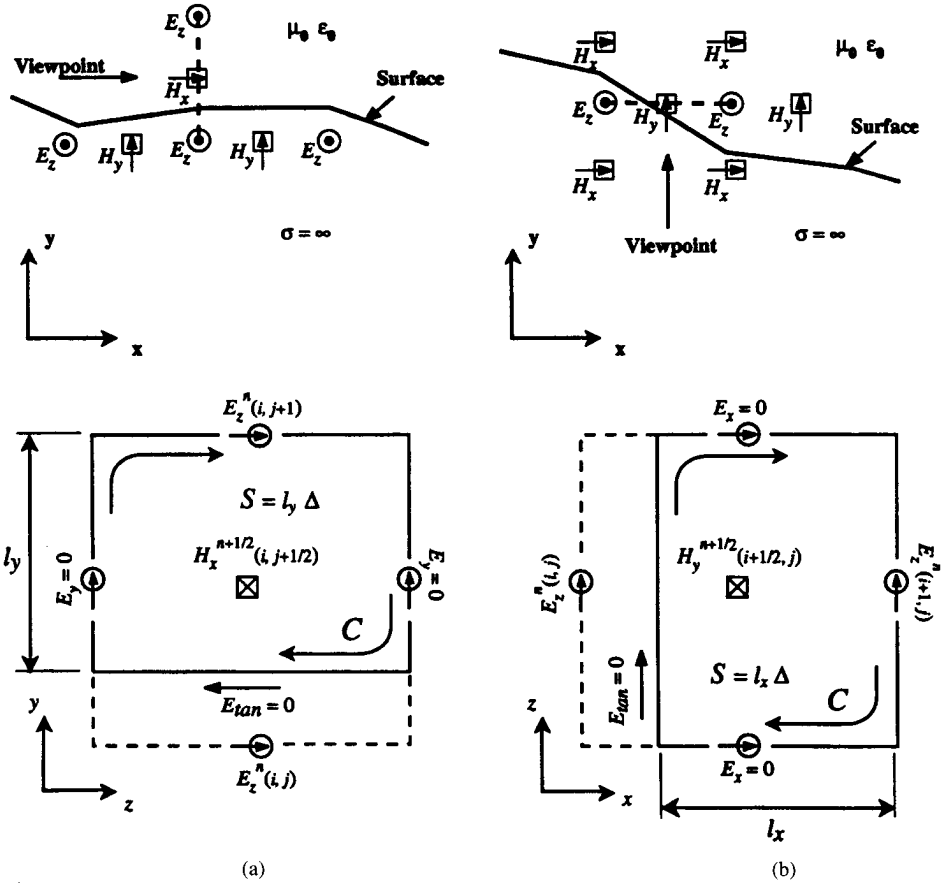

Fig. 3. Two views of the Faraday contour truncation. Orientations are specified by the adjoining axes. (a) Contour for finding $H_x^{n+(1/2)}(i, j + \frac{1}{2})$. (b) Contour for finding $H_y^{n+(1/2)}(i + \frac{1}{2}, j)$. The latter contour can also be truncated on the opposite side.

If the path were truncated on the right side, (11) would be the appropriate equation.

Unfortunately, (7) cannot be used to compute E_z-field components which have truncated Ampere contours; the tangential H-field is not known along the surface and is, therefore, unknown along part of the Ampere contour shown in Fig. 4. Hence, these E_z-field values are not used, and H_x and H_y values dependent on the unused E_z-grid points must also be computed using (9)–(11). For such cases, l_x and l_y are extended beyond one grid space to reach the surface. It should be emphasized that (9)–(11) are used only along the surface; the UFDTD equations are used elsewhere. The implementation is straightforward and does not add significantly to the computational cost.

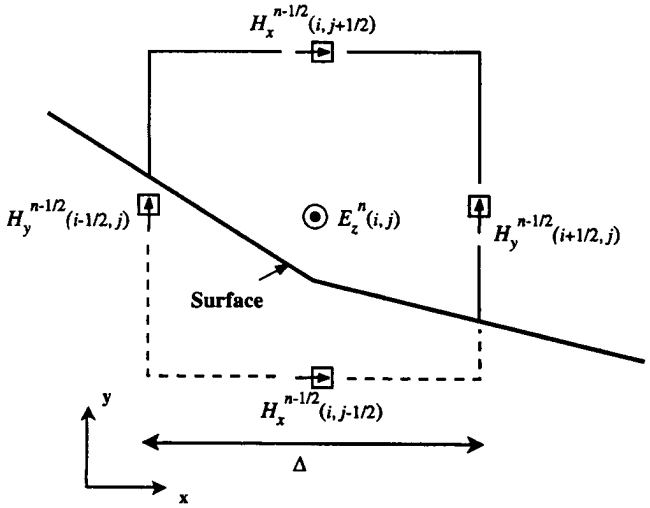

Fig. 4. Illustration of a truncated Ampere contour.

C. Absorbing Boundary Conditions

Rough surface scattering is by nature an unbounded problem. FDTD simulations, however, must be restricted to a finite computational domain such as the one shown in Fig. 1. The resulting boundaries present a problem. This can be seen if we attempt to evaluate (4)–(6) for the edge grid points. By construction, the $\boldsymbol{H}$-field points have the necessary adjacent field points for their computation, but the $\boldsymbol{E}$-field points lack at least one neighboring $\boldsymbol{H}$-field component. This deficiency indicates that the basic FDTD equations cannot be used alone to model an unbounded scattering problem. A standard solution is to use auxiliary equations for the boundary points. These equations, known as absorbing boundary conditions (ABC's), force the E_z values at the edges of the grid to behave as if no boundary exists. The scattered field is, in effect, absorbed as it radiates onto the grid boundary. Since the ABC's are imperfect, however, nonphysical reflections can occur that significantly reduce the performance of the FDTD method.

For this work, both the modified third-order Liao ABC [30], [31] with superabsorption [19] and the perfectly matched layer (PML) ABC [32]–[34] were used. Both approaches gave similar performance, but because the PML ABC is easier to implement, it was used for the examples presented. For the PML ABC, the FDTD grid is enclosed within a perfectly matched layer 16 grid cells deep. This layer simulates a lossy material that is impedance matched to the free space medium of the grid interior. Flat buffer zones are included at the surface edges to provide space for the PML, and the incident field is set to zero within these zones.

D. The Incident Field

In numerical simulations of rough surface scattering, finite-length surfaces must be used to model scattering from infinite surfaces. When a single plane wave strikes a finite-length surface, edge diffraction occurs. One way of minimizing diffraction effects is to construct an incident wave that tapers to very small values at the surface edges. Diffraction still occurs, but it makes negligible contributions to the scattered field.

Tapered incident waves have been introduced by Thorsos [35] and Chan and Fung [36]. The tapered incident field used by Thorsos is an approximation to an incident field, consisting of an angular spectrum of plane waves, that satisfies the wave equation exactly. Presented in a form consistent with Fig. 1, the field is given by

$$E_z^i(\boldsymbol{r}) = \exp\{-j\boldsymbol{k}_i \cdot \boldsymbol{r}[1 + w(\boldsymbol{r})] - (x - y\tan\theta_i)/g^2\} \quad (12)$$

where

$$w(\boldsymbol{r}) = [2(x - y\tan\theta_i)^2/g^2 - 1]/(kg\cos\theta_i)^2 \quad (13)$$

$\boldsymbol{r} = (x, y)$ is a point above the surface, θ_i is the incident angle measured from the vertical, and $\boldsymbol{k}_i = k(\sin\theta_i, -\cos\theta_i)$ is the incident wave vector in the x-y plane. The phasor expression in (12) is implemented in its time-dependent form for $t \geq 0$. Equation (12) satisfies the wave equation to order $1/(kg\sin\theta_i)^2$ for $kg\sin\theta_i \gg 1$. The parameter g controls the tapering, and care must be taken in its choice. Angular resolution, edge effects, and accuracy in satisfying the wave equation all depend on g [35]. In addition, for the Monte-Carlo results to be useful for testing the validity of approximate rough surface scattering models, the tapering must be accomplished in such a way that differences between the finite surface, tapered plane wave results and infinite surface, single plane wave results are negligible. For the numerical examples presented in this paper, $g = L/4$ and $L/4.5$ are used, where L is the horizontal extent of each surface.

To reduce transients caused when the incident field is turned on, (12) is multiplied by a ramp of the form $1 - \exp(-g_t t^2)$. The constant g_t is chosen such that the field is one-half its maximum amplitude five cycles after the incident field is switched on. This value of g_t yields an incident field with a narrow bandwidth. The use of this ramp significantly reduces the time needed to converge to steady state.

E. Surface Generation

For each numerical study, 50 finite-length surfaces are generated using the method proposed by Thorsos [35]; equations are given here for completeness. We wish to generate surfaces $f(x)$ that satisfy either a Gaussian or Pierson–Moskowitz surface roughness spectrum. The general procedure is to randomly generate a surface spectrum that has Gaussian statistics and then inverse transform the spectrum to obtain a surface profile. This approach produces Gaussian distributed heights and slopes for either of the two spectra. Each surface consists of N discrete points spaced Δx apart over a surface length L. Horizontal locations are specified by $x_n = n\Delta x$ for $1 \leq n \leq N$. The surfaces are generated using [35]

$$f(x_n) = \frac{1}{L}\sum_{\ell=-N/2}^{N/2-1} F(K_\ell)\exp[-jK_\ell x_n] \quad (14)$$

where, for $\ell \geq 0$

$$F(K_\ell) = \sqrt{2\pi L W(K_\ell)} \cdot \begin{cases} \frac{1}{\sqrt{2}}[N(0,1) - jN(0,1)] & \\ \qquad\qquad \text{for } 1 \leq \ell \leq N/2 - 1 & \\ N(0,1) \qquad \text{for } \ell = 0, N/2 & \end{cases} \quad (15)$$

and for $\ell < 0, F(K_{-\ell}) = F(K_\ell)^*$. In (15), we use either a Gaussian or Pierson–Moskowitz surface roughness spectrum. For the Gaussian spectrum

$$W(K_\ell) = \frac{h^2 l}{2\sqrt{\pi}}\exp[-K_\ell^2 l^2/4] \quad (16)$$

where $K_\ell = 2\pi\ell/L$, h is the rms surface height, l is the correlation length, and $N(0,1)$ is a number sampled from a Gaussian distribution with zero mean and unity variance. For the Pierson–Moskowitz spectrum [29]

$$W(K_\ell) = \frac{\alpha}{4|K_\ell|^3}\exp[-(\beta g_c^2)/(K_\ell^2 U^4)] \quad (17)$$

where $\alpha = 0.0081$, $\beta = 0.74$, $g_c = 9.81$, $\mathrm{m/s^2}$, and U is the wind speed specified at a height of 19.5 m above the surface mean.

The nature of the discrete spectrum causes correlation of the ends of each surface. To circumvent this, an extended surface much longer than the N required points is generated. Each surface realization used is then cut from the longer surface so correlation is negligible. For the numerical examples presented in Section III, each surface of length L is taken from a surface with total length L' which is at least 20 correlation lengths longer than L.

Surfaces generated as described above potentially have different statistical properties when used in the UFDTD algorithm. For the UFDTD algorithm, space is partitioned into a uniform Cartesian grid, and surface heights are "quantized" to coincide with grid points. This produces a modified surface with a vertically discrete, stair-stepped appearance, with each step equal to an integral number of grid spaces. We wish to know if the quantization of the surface heights affects the statistical parameters so that they differ from those of the continuous surface realizations. The relative statistical accuracy of

the two different types of surface realizations—that is, continuous and vertically discrete—can be determined by estimating rms heights and correlation lengths. Using the definitions for the mean square surface height $h^2 = \langle (f(x) - \langle f(x) \rangle)^2 \rangle$ and the correlation function $B_f(x, x_0) = \langle f(x) f(x+x_0) \rangle$—where x_0 is the horizontal distance between surface points, x is the absolute location, and the angle brackets indicate averaging over the surface—correlation lengths and rms surface heights were computed for 50 Monte-Carlo surface realizations for a Gaussian spectrum. These data show that variations in the statistical parameters of the continuous and vertically discrete generated surfaces are typically less than 1%.

F. Far-Field Conversion and Monte-Carlo Averaging

The UFDTD and CPFDTD results presented in the next section are given in terms of the bistatic radar cross section. The bistatic radar cross section for a plane wave incident on a 1-D surface is [37]

$$\sigma(\theta_s, \theta_i) = 2\pi \frac{I_s \rho}{I_i L} \tag{18}$$

where ρ is the distance to the far-field observation point, L is the length of the surface, I_s is the scattered intensity, I_i is the incident intensity, θ_s is the angle of observation measured from the vertical, and θ_i is the angle of incidence measured from the vertical. To find the bistatic radar cross section, it is necessary to convert near-field values to far-field values.

For each surface realization, far-field values are found as described in [5] using source equivalence concepts. It can be shown that

$$I_s = \frac{k}{8\pi\rho} \int_0^{L_x} dx[-\cos\theta_s E_z(x, L_y) + c\mu H_x(x, L_y)] \times \exp\{-jk(L_y \cos\theta_s - x \sin\theta_s)\} \tag{19}$$

where $E_z(x, L_y)$ and $H_x(x, L_y)$ are field values found as shown in Fig. 5. Along the dashed path in this figure phasor quantities for E_z and H_x are obtained from the FDTD algorithm. For our choice of path, E_z is averaged between grid points, and a correction must also be made for the fact that the electric field is available at a different time than the magnetic field. In (19), ρ is as shown in Fig. 5(b), μ and c are the permeability and speed of light in free space, and k is the radiation wavenumber. The observation angle is given by $\theta_s = 90$ degrees $- \phi$ for the angle ϕ shown in Fig. 5(b). Note that (19) utilizes only the field values collected on the horizontal portion of the dashed path; the contributions from the vertical edges of the path are neglected. This is a reasonable approximation since the field is smallest at the surface edges, and the length of the discarded portion is a small percentage of the length of the total integration path. An alternate approach used by Lee *et al.* [38] is also available for finding far fields.

Equation (19) is further modified to include the effects of numerical dispersion present on the FDTD grid. This dispersion causes a wave traveling on the grid to have a speed which is slower than its theoretical speed in free space. For CW illumination, the amount of dispersion depends on the number of grid ppw and the direction of propagation. A dispersion curve can be obtained [6] which gives the ratio v_p/c as a function of propagation angle for a fixed ppw where v_p is the phase velocity on the FDTD grid and c is the speed of light in free space. A modified k given by $k_{\text{mod}} = k/(v_p/c)$ is used in (19), where the value of v_p is chosen to match propagation at the incident angle. This choice is based on the assumption that most of the scattered energy is in the specular direction. In addition, it is necessary to use k_{mod} in the incident field (12) to accurately couple the incident energy into the grid and to produce the correct specular scattering angle. Finally, to match the surface geometry to the shortened wavelength of the computed field, a reduced wavelength $\lambda_r = \lambda(v_p/c)$ is used in the surface generation process. These changes permit the use of a sparser FDTD grid, thereby reducing computational cost.

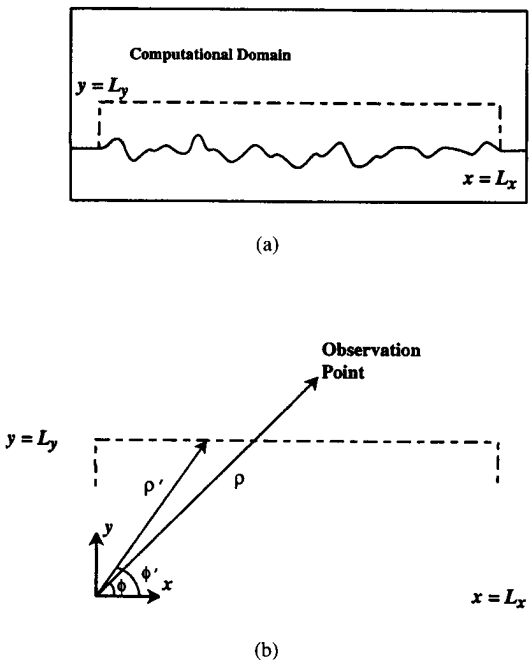

Fig. 5. (a) Computational domain in which the scattered fields propagate. (b) Contour over which currents are found from the scattered field to obtain far-field results.

Equation (19) is used in (18) to compute the radar cross section. Using energy flux through the surface produced by the tapered incident field (12), it can be shown that [35]

$$\sigma(\theta_s, \theta_i) = \frac{2\sqrt{2\pi} I_s \rho}{g[1 - 0.5(1 + 2\tan^2\theta_i)/(kg\cos\theta_i)]}. \tag{20}$$

The Monte-Carlo results for the bistatic radar cross section are obtained by averaging the results over 50 surface realizations.

III. Numerical Results

In this section, the results of the Monte-Carlo simulations are presented. For the Gaussian roughness spectrum, four incident angles are considered. Two grazing incidence cases are shown for the Pierson–Moskowitz spectrum. The total bistatic radar cross sections, both coherent and incoherent parts, are plotted as a function of the scattering angle. Fluctuations in the results are due to the finite number of surface realizations used in the Monte-Carlo ensemble average. Dispersion correction, as discussed in Section II-F, has been included

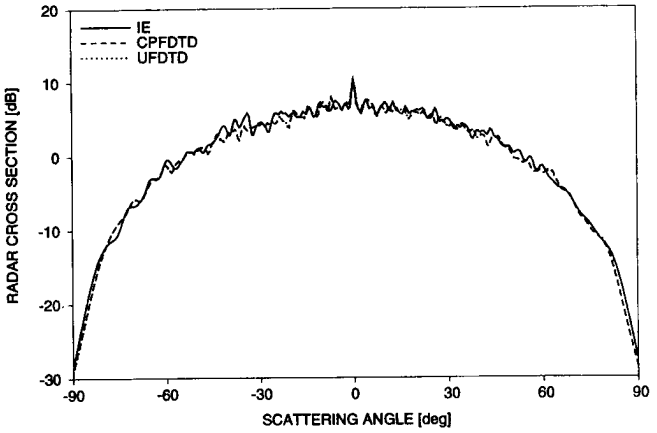

Fig. 6. IE, UFDTD, and CPFDTD radar cross section results for a Gaussian roughness spectrum and normal incidence. Surface parameters are $kh = 1$, $kl = 4.24$, and $\gamma = 18.4$ degrees.

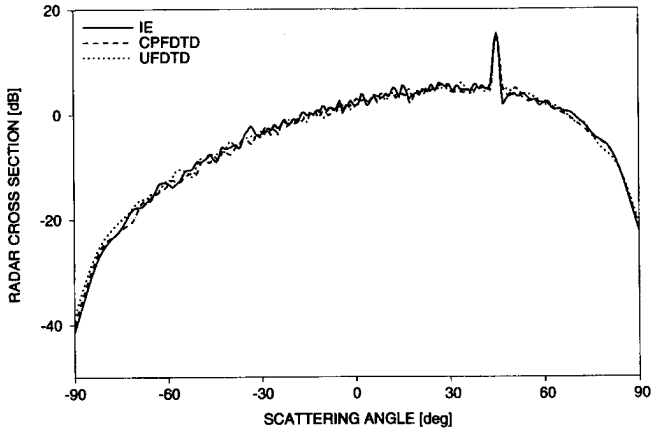

Fig. 7. For the same comparison, the incident angle has been increased to 45 degrees.

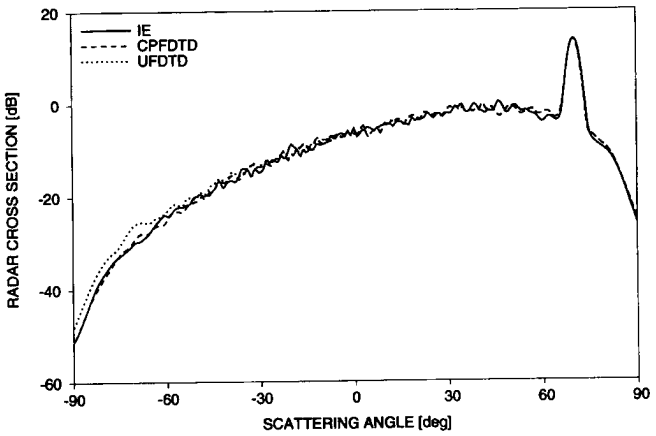

Fig. 8. For the same comparison, the incident angle has been increased to 70 degrees.

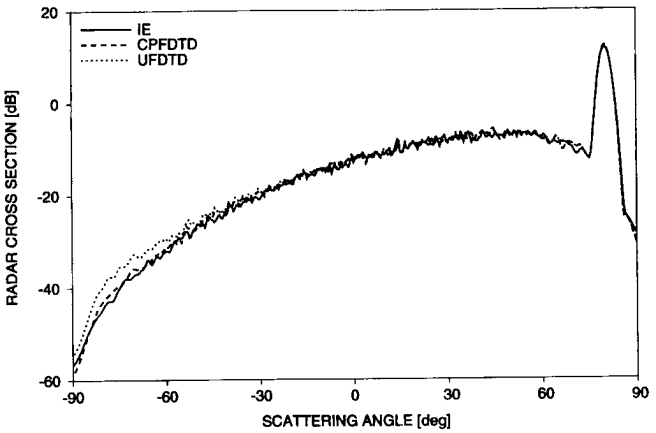

Fig. 9. For the same comparison, the incident angle has been increased to 80 degrees.

in all results shown. For the examples studied, it was found that the CPFDTD method gives no significant enhancement for incident angles less than 45 degrees. Hence, UFDTD is sufficient for the smaller angles. Results were obtained using desktop workstations.

In Figs. 6–9 we compare integral equation (IE) results provided by Thorsos [35] with UFDTD and CPFDTD results calculated at 16 ppw. The surface roughness parameters are $kh = 1.00$, $kl = 4.24$, and $\gamma = 18.4$ degrees where k is the radiation wavenumber, h is the rms surface height, l is the correlation length, and γ is the rms surface slope angle. This surface is fairly rough as indicated by the small specular peak. For incident angles up to 70 degrees, we use 80λ surfaces, but we increase this value to 160λ for 80 degrees incidence. In Fig. 6 we see that the agreement with IE results is good for both the UFDTD and CPFDTD methods. Hence UFDTD is sufficient for this case. In Fig. 7 the same comparison is made for $\theta_i = 45$ degrees. Once again it is apparent that UFDTD is in agreement over most angles with the IE results; however, a slight overprediction is beginning to occur in the grazing backscatter direction. In Figs. 8 and 9 we increase the incident angles to 70 degrees and 80 degrees, respectively, for the same surface parameters. For these cases the CPFDTD method offers enhanced performance.

In Figs. 10 and 11, scattering is calculated for a Pierson–Moskowitz spectrum with $kh = 1.79$ where $h = \alpha U^4/(4\beta g_c^2)$ and U is the wind speed in m/s. In these figures, the incident angles are $\theta_i = 70$ degrees and $\theta_i = 80$ degrees, respectively. The surfaces are 180λ long, and the incident field taper factor is $g = L/4.5$. The IE and 16 ppw CPFDTD results are in good agreement.

IV. Summary

An implementation of the FDTD algorithm incorporating the contour path method is used to develop a Monte-Carlo technique for wave scattering from rough surfaces. Results for the bistatic radar cross section are presented for the Dirichlet boundary condition for 1-D surfaces with Gaussian statistics satisfying a Gaussian roughness spectrum and for surfaces satisfying a Pierson–Moskowitz spectrum. Angles of incidence in the range 0 degrees $\leq \theta_i \leq$ 80 degrees are considered. The results show the CPFDTD method provides improved performance over the UFDTD method for incident angles greater than 45 degrees.

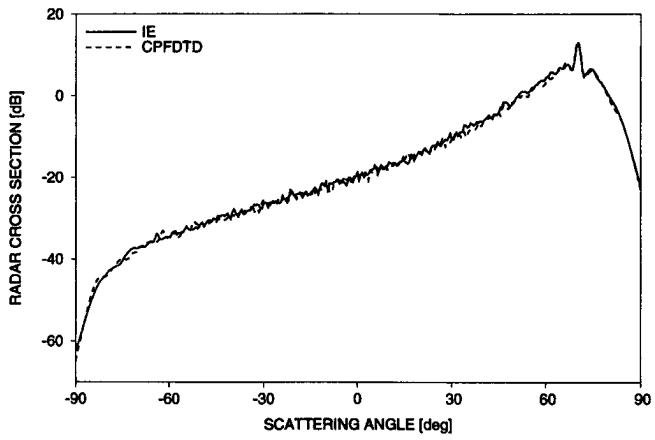

Fig. 10. IE versus CPFDTD using a Pierson–Moskowitz spectrum with U = 20 m/s, θ_i = 70 degrees.

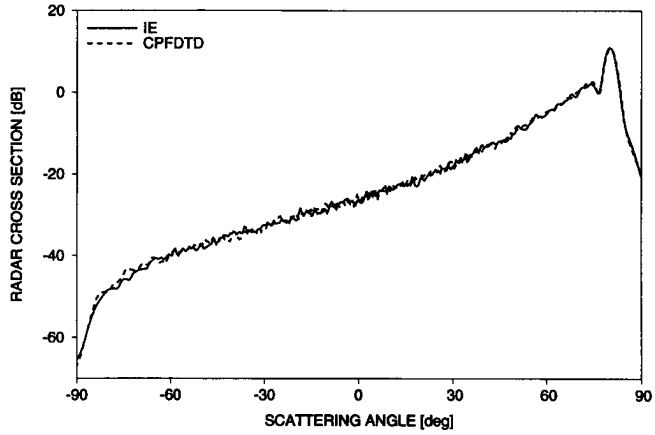

Fig. 11. IE versus CPFDTD using a Pierson–Moskowitz spectrum with U = 20 m/s, θ_i = 80 degrees.

In future work, we will consider a combination of volume and surface scattering geometries as well as penetrable surfaces. The CPFDTD method will be used to study these problems directly, but it will also be used to benchmark approximate stochastic models.

ACKNOWLEDGMENT

The authors would like to thank Dr. E. I. Thorsos of the Applied Physics Laboratory, College of Ocean and Fishery Sciences, University of Washington, Seattle, WA, for use of the Monte-Carlo integral equation results.

REFERENCES

[1] K. S. Yee, "Numerical solution of initial boundary value problems involving Maxwell's equations in isotropic media," *IEEE Trans. Antennas Propagat.*, vol. AP-14, no. 4, pp. 302–307, 1966.

[2] A. Taflove and M. E. Brodwin, "Numerical solution of steady-state electromagnetic scattering problems using the time-dependent {Maxwell's} equations," *IEEE Trans. Microwave Theory Tech.*, vol. MTT-23, no. 8, pp. 623–630, 1975.

[3] G. Mur, "Absorbing boundary conditions for the finite-difference approximation of the time-domain electromagnetic-field equations," *IEEE Trans. Electromagnetics Compat.*, vol. EMC-23, no. 4, pp. 377–382, 1981.

[4] Z. P. Liao, H. L. Wong, B.-P. Yang, and Y.-F. Yuan, "A transmitting boundary for transient wave analysis," *Sci. Sin., Ser. A*, vol. 27, no. 10, pp. 1063–1076, 1984.

[5] K. R. Umashankar and A. Taflove, "A novel method to analyze electromagnetic scattering of complex objects," *IEEE Trans. Electromagnetics Compat.*, vol. EMC-24, no. 4, pp. 397–405, 1982.

[6] A. Taflove, "Review of the formulation and applications of the finite-difference time-domain method for numerical modeling of electromagnetic wave interactions with arbitrary structures," *Wave Motion*, vol. 10, no. 6, pp. 547–582, 1988.

[7] A. Taflove and K. R. Umashankar, "The finite-difference time-domain (FDTD) method for electromagnetic scattering and interaction problems," *J. Electromagnetic Waves Appl.*, vol. 1, no. 4, pp. 363–387, 1987.

[8] K. S. Kunz and R. J. Luebbers, *The Finite Difference Time Domain Method for Electromagnetics*. Boca Raton, FL: CRC Press, 1993.

[9] C. H. Chan, S. H. Lou, L. Tsang, and J. A. Kong, "Electromagnetic scattering of waves by rough surfaces: A finite-difference time-domain approach," *Microwave Opt. Technol. Lett.*, vol. 4, no. 9, pp. 355–359, 1991.

[10] C. H. Chan, L. Li, J. T. Elson, and L. Tsang, "A conformal finite-difference time-domain approach for monte carlo simulations of random rough surface scattering," in *Proc. URSI Dig.*, Chicago, IL, July 1992, p. 13.

[11] T. G. Jurgens, A. Taflove, K. Umashankar, and T. G. Moore, "Finite-difference time-domain modeling of curved surfaces," *IEEE Trans. Antennas Propagat.*, vol. 40, no. 4, pp. 357–366, 1992.

[12] N. K. Madsen and R. W. Ziolkowski, "Numerical solution of Maxwell's equations in time domain using irregular nonorthogonal grids," *Wave Motion*, vol. 10, no. 6, pp. 583–596, 1988.

[13] K. S. Yee, J. S. Chen, and A. H. Chang, "Conformal finite-difference time-domain (FDTD) with overlapping grids," *IEEE Trans. Antennas Propagat.*, vol. 40, no. 9, pp. 1068–1075, 1992.

[14] V. Shankar, W. F. Hall, and A. Mohammadian, "A time-domain differential solver for electromagnetic scattering problems," in *Proc. IEEE*, vol. 77, no. 5, pp. 709–721, 1989.

[15] M. Fusco, "FDTD algorithm in curvilinear coordinates," *IEEE Trans. Antennas Propagat.*, vol. 38, no. 1, pp. 76–89, 1990.

[16] R. Holland, "Finite difference solutions of Maxwell's equations in generalized nonorthogonal coordinates," *IEEE Trans. Nucl. Sci.*, vol. NS-30, no. 6, pp. 4589–4591, 1983.

[17] B. J. McCartin and J. F. Dicello, "Three-dimensional finite difference frequency domain scattering using the control region approximation," *IEEE Trans. Magnetics*, vol. 25, pp. 3092–3097, 1989.

[18] S. L. Ray, "Numerical dispersion and stability characteristics of time-domain methods on nonorthogonal meshes," *IEEE Trans. Antennas Propagat.*, vol. 41, no. 2, pp. 233–235, 1993.

[19] K. K. Mei and J. Fang, "Superabsorption—A method to improve absorbing boundary conditions," *IEEE Trans. Antennas Propagat.*, vol. 40, no. 9, pp. 1001–1010, 1992.

[20] S. H. Lou, L. Tsang, C. H. Chan, and A. Ishimaru, "Monte Carlo simulations of scattering of waves by a random rough surface with the finite element method and the finite difference method," *Microwave Opt. Technol. Lett.*, vol. 3, no. 5, pp. 150–154, 1990.

[21] S. H. Lou, L. Tsang, and C. H. Chan, "Application of the finite element method to Monte Carlo simulations of scattering of waves by random rough surfaces: Penetrable case," *Waves in Random Media*, vol. 1, pp. 287–307, 1991.

[22] L. Tsang, S. H. Lou, C. H. Chan, and A. Ishimaru, "Application of the finite element method to Monte Carlo simulations of scattering of waves by random rough surfaces with the periodic boundary condition," *J. Electromagnetic Waves Appl.*, vol. 5, no. 8, pp. 835–855, 1991.

[23] L. Tsang, S. H. Lou, and C. H. Chan, "Application of the extended boundary condition method to Monte Carlo simulations of scattering of waves by two-dimensional random rough surfaces," *Microwave Opt. Technol. Lett.*, vol. 4, no. 12, pp. 527–531, 1991.

[24] R. Devayya and D. H. Wingham, "The numerical calculation of rough surface scattering by the conjugate gradient method," *IEEE Trans. Geosci. Remote Sensing*, vol. 30, no. 3, pp. 645–648, 1992.

[25] A. K. Fung, M. R. Shah, and S. Tjuatja, "Numerical simulation of scattering from three-dimensional randomly rough surfaces," *IEEE Trans. Geosci. Remote Sensing*, vol. 32, no. 5, pp. 986–994, 1994.

[26] J. B. Schneider and S. L. Broschat, "Wave scattering from perfectly conducting surfaces using the FDTD method," in *URSI Radio Sci. Meet. Dig.*, Chicago, IL, July 1992, p. 14.

[27] F. D. Hastings, S. L. Broschat, and J. B. Schneider, "An application of the contour path finite-difference time-domain method to rough surface scattering," in *Proc. URSI Radio Sci. Meet.*, Ann Arbor, MI, June 1993.

[28] ——, "The FDTD method for scattering from rough surfaces: Oblique incidence," in *Proc. URSI Radio Sci. Meet.*, Seattle, WA, June 1994, p. 372.
[29] E. I. Thorsos, "Acoustic scattering from a "Pierson–Moskowitz" sea surface," *J. Acoust. Soc. Am.*, vol. 88, pp. 335–349, 1990.
[30] W. C. Chew, *Waves and Fields in Inhomogeneous Media.* New York: Van Nostrand Reinhold, 1990, pp. 235–256.
[31] W. C. Chew and R. L. Wagner, "A modified form of Liao's absorbing boundary condition," in *Proc. IEEE Antennas and Propagat. Soc. Int. Symp.*, Chicago, IL, vol. 1, pp. 536–539, July 1992.
[32] J. P. Berenger, "A perfectly matched layer for the absorption of electromagnetics waves," *J. Comput. Phys.*, vol. 114, no. 1, pp. 185–200, 1994.
[33] D. S. Katz, E. T. Thiele, and A. Taflove, "Validation and extension to three dimensions of the Berenger PML absorbing boundary condition for FD-TD meshes," *IEEE Microwave Guided Wave Lett.*, vol. 4, no. 8, pp. 268–270, 1994.
[34] C. E. Reuter, R. M. Joseph, E. T. Thiele, D. S. Katz, and A. Taflove, "Ultrawideband absorbing boundary condition for termination of waveguiding structures in FD-TD simulations," *IEEE Microwave Guided Wave Lett.*, vol. 4, no. 10, pp. 344–346, 1994.
[35] E. I. Thorsos, "The validity of the Kirchhoff approximation for rough surface scattering using a Gaussian roughness spectrum," *J. Acoust. Soc. Am.*, vol. 83, pp. 78–92, 1988.
[36] H. L. Chan and A. K. Fung, "A numerical study of the Kirchhoff approximation in horizontally polarized backscattering from a random surface," *Radio Sci.*, vol. 13, no. 5, pp. 811–818, 1978.
[37] A. Ishimaru, *Wave Propagation and Scattering in Random Media.* New York: Academic, 1978.
[38] S. M. Lee, W. C. Chew, M. Moghaddam, M. A. Nasir, S.-L. Chuang, R. W. Herrick, and C. L. Balestra, "Modeling of rough-surface effects in an optical turning mirror using the finite-difference time-domain method," *J. Lightwave Technol.*, vol. 9, no. 11, pp. 1471–1480, 1991.

Frank D. Hastings (S'90–M'92) received the B.S. summa cum laude and M.S. degrees in electrical engineering from Washington State University, Pullman, in 1991 and 1993, respectively. He is currently working towards his Ph.D. in electrical engineering at the same university.

His research interests include rough surface scattering and computational techniques in electromagnetics and acoustics.

Mr. Hastings is the recipient of the Curtis, Boeing, and Suksdorf Fellowships.

John Schneider (M'92) received the B.S. degree in electrical engineering summa cum laude from Tulane University, New Orleans, LA, and the M.S. and Ph.D. degrees in electrical engineering from the University of Washington, Pullman.

He is presently an Assistant Professor in the School of Electrical Engineering and Computer Science at Washington State University, Pullman. His current research interests include numerical methods in electromagnetics and acoustics.

Shira Lynn Broschat (S'81–M'89) received the B.S., M.S., and Ph.D. degrees in electrical engineering from the University of Washington in Seattle.

From 1983 to 1985 she was a Research Associate for the Bioelectromagnetics Research Laboratory at the University of Washington, Seattle, where she did work on microwave hyperthermia treatment of cancer. From 1985 to 1989 she was a research associate at the University of Washington's Applied Physics Laboratory where she was involved in research on wave scattering from rough surfaces. In 1989 she became an Assistant Professor at Washington State University in Pullman, WA, where she is currently an Associate Professor in the School of Electrical Engineering and Computer Science. Her current research interests include rough surface scattering, ultrasound imaging, remote sensing, and engineering education.

Dr. Broschat is a member of the IEEE Geoscience and Remote Sensing Society, the Optical Society of America, the Acoustical Society of America, Radio Science (Commission B), and Tau Beta Pi. She is the recipient of a Young Investigator Award from the Office of Naval Research, a Presidential Young Investigator Award from the National Science Foundation, and a Presidential Faculty Fellows Award from the National Science Foundation.